



Preparation, characterization, and iodide sorption performance of silver-loaded mesoporous MCM-41

Noredin Karkhanei^a, Hamid Sepehrian^{b,*}, Ramin Cheraghali^a

^aChemistry Department, Islamic Azad University, Saveh Branch, Saveh, Iran, Tel. +98 9353628877; email: noredin.karkhanei@gmail.com (N. Karkhanei), Tel. +98 9122936072; email: ramin.cheraghali@yahoo.com (R. Cheraghali)

^bNuclear Science and Technology Research Institute, AEOL, P.O. Box 11365/8486, Tehran, Iran, Tel. +98 2188221117; Fax: +98 2188221116; email: hsepehrian@aeoi.org.ir (H. Sepehrian)

Received 7 December 2013; Accepted 5 September 2014

ABSTRACT

Mesoporous MCM-41 has been modified by incipient wetness impregnation with silver atoms as a new sorbent for iodide. The Ag-modified mesoporous MCM-41 (Ag-MCM-41) was characterized using X-ray diffraction, surface area, pore volume and pore size analyzer, and scanning electron microscopy/energy dispersive spectroscopy techniques, and its sorption behavior for iodide was studied. The effects of pH, contact time, temperature, initial concentration of iodide, and competing anions such as chloride and fluoride were investigated by batch method. The sorption capacity was very high in the pH range of 1.0–3.0. The kinetic analysis revealed that the overall sorption process was fitted with the pseudo-second-order kinetic model. The experimental sorption isotherm is also successfully described by Langmuir and Freundlich models. The maximum sorption capacity of iodide onto Ag-MCM-41 was found to be 238.1 mg g⁻¹.

Keywords: Mesoporous MCM-41; Impregnation; Silver; Iodide sorption

1. Introduction

The presence of iodide (I⁻) in source waters can result in the formation of iodinated disinfection by-products upon exposure to natural organic matter and disinfectant, which are often more toxic than their chlorinated analogues [1–5].

On the other hand, ¹²⁹I is a particularly long-lived isotope (half-life of 1.57 × 10⁷ years) that must be captured and reliably stored while it decays, whereas the ¹³¹I is short-lived isotope (half-life of 8.02 d) but requires immediate capture because it directly affects human metabolic processes [6]. As a result of defects

in fuel elements, radioactive iodine (radioiodine) gets into the primary circuit coolant during the operating period in nuclear power plants. Radioiodine may be present in ionic forms in the primary circuit solution, I⁻, IO⁻, and IO³⁻ as well as in the form of molecular iodine, I₂ [7].

Numerous materials, including silver-impregnated sorbents (e.g. zeolite and alumina), activated carbons, activated carbon fibers, and anion-exchange resins, have been evaluated for use in removal of iodide from the aqueous phase [8,9]. Organic resins have been applied to remove anionic species from radioactive wastewaters. However, they are not recommended for practical application as sorbent because of their radiolytic decomposition. As an alternative inorganic

*Corresponding author.

anion-exchange material, hydrotalcites have been proposed [10].

The mesoporous silicate molecular sieves, due to their high surface area, have found good use as catalyst [11,12] and efficient adsorbent [13–15]. Incorporation of organic and inorganic modifiers into the framework of mesoporous molecular sieves makes them more efficient catalyst for selective oxidation and as potential sorbent for selective separations.

The mesoporous silicate MCM-41 and its modified forms have been used because of large specific surface area, large pore volume and cylindrical pores, with a uniform pore distribution as new adsorbents in recent years [16,17]. On the other hand, modification of these adsorbents by inorganic modifiers unlike organic modifiers is a rapid, simple, and inexpensive method.

In this paper, mesoporous MCM-41 has been modified by incipient wetness impregnation with silver atoms as new sorbent for iodide. The effects of pH, contact time, temperature, initial concentration of iodide, and competing anions such as chloride and fluoride have been investigated by batch method.

2. Experimental

2.1. Reagents

In our experiments, all the reagents were analytical grade and used without further purification. All the reagents used were purchased from Merck (Darmstadt, Germany), except cetyltrimethylammonium bromide (CTAB) which was supplied by Aldrich (Milwaukee, WI, USA).

2.2. Preparation of silver-modified mesoporous MCM-41

Mesoporous MCM-41 was prepared according to our published papers previously [18]. After the preparation of mesoporous MCM-41, monolayer AgNO₃-MCM-41 was prepared by incipient wetness impregnating MCM-41 with an appropriate amount of aqueous solution of silver nitrate (AgNO₃). The weight ratio of silver nitrate to the MCM-41 was 0.60, based on estimate for monolayer spreading of AgNO₃. First, a 1.2 mol L⁻¹ solution of AgNO₃ was prepared. A volume of solution equal to the total pore volume of sample was introduced and mixed with the MCM-41 so that a weight ratio of 0.60 was achieved. Then, the sample was heated for 12 h at 105°C in air to remove the water [19].

Finally, the AgNO₃-MCM-41 sample was modified by treatment with a 10 mol L⁻¹ solution of hydrazine hydrate (solid to solution ratio was 0.05 g mL⁻¹). The process was performed at room temperature for 1 h.

The sorbent was separated from the mother liquor by filtration, washed with water, and dried in air for 24 h at 100°C. The prepared sample was labeled as Ag-MCM-41.

2.3. Sorbent characterization

Characterization of the prepared Ag-MCM-41 was performed by powder X-ray diffraction (XRD), surface area, pore volume and pore size analyzer, and scanning electron microscopy/energy dispersive spectroscopy (SEM/EDS) techniques. A Philips X'pert powder diffractometer system with Cu-K α ($\lambda = 1.541 \text{ \AA}$) radiation was used for X-ray studies. XRD analysis was performed from 1.5° to 100° (2θ) at a scan rate of 0.02° (2θ) s⁻¹. A Quantachrome NOVA 2200e instrument was used for the determination of the physical properties such as surface area, pore volume, and pore size. A Philips XL-30 SEM associated with EDS was also used for surface morphology studies and chemical components analysis of the prepared sample. Point of zero charge was determined by pH drift method [20,21]. A 0.01 mol L⁻¹ KNO₃ was used as inert electrolyte. The pH of test solutions were adjusted in range between 2 and 10 using 0.01 mol L⁻¹ HNO₃ and 0.01 mol L⁻¹ KOH. A 0.2 g of the Ag-MCM-41 adsorbents were added to 50 mL of test solutions into stopped glass tubes and equilibrated for 24 h. The final pH (pH_f) was measured after 24 h and plotted against the initial pH (pH_i). The pH where the curve intersects the line pH_i = pH_f was taken as the pH_{pzc}. pH was measured by Schott CG841 pH-meter (Germany), which was calibrated before every measure.

2.4. Sorption studies

The sorption studies of the iodide on the Ag-MCM-41 sorbent were carried out using a batch method [22]. In this procedure, 25 mg of sorbent was dispersed in 25 mL solution with different concentrations of the iodide ion (88–352 mg L⁻¹). The mixture was shaken at 150 rpm for 0.5–48 h using a water shaker bath at temperatures of 25–65°C. Then the Ag-MCM-41 was removed by filtration, and the iodide concentration of the filtrate was measured by inductively coupled plasma atomic emission spectroscopy. The percent removal (R , %), the adsorption amount (q , mg g⁻¹), and the distribution coefficient (k_d , mL g⁻¹) were calculated using Eqs. (1–3), respectively.

$$R = \frac{(C_i - C_f)}{C_i} \times 100 \quad (1)$$

$$q = (C_i - C_f) \times \frac{V}{m} \quad (2)$$

$$k_d = \frac{(C_i - C_f)}{C_f} \times \frac{V}{m} \quad (3)$$

where C_i and C_f are the initial and residual concentrations (mg L^{-1}) of iodide, V is the total volume of iodide solution (mL), and m is the mass of the sorbent used (g).

2.4.1. Effect of the solution pH

The effect of the solution pH on the adsorption behavior was determined at a constant temperature of 25°C for 48 h. In batch experiments, 25 mg of the Ag-MCM-41 adsorbent was equilibrated with 25 mL

of the solution containing $1.2 \times 10^{-2} \text{ mol L}^{-1}$ of iodide ions at various pH values. The pH was adjusted with $0.01 \text{ mol L}^{-1} \text{ HNO}_3$ and $0.01 \text{ mol L}^{-1} \text{ KOH}$ in the pH range of 1.0–8.0.

2.4.2. Effect of contact time

In a typical kinetic test, 25 mg of the Ag-MCM-41 adsorbent was added to 25 mL of $1.2 \times 10^{-2} \text{ mol L}^{-1}$ iodide solution at pH 2.0. The suspension was agitated for different periods of time (from 30 min to 48 h) using a water bath shaker.

2.4.2.1. Kinetic modeling. In order to investigate the controlling mechanism of adsorption processes such as mass transfer and chemical reaction, the pseudo-first-order and pseudo-second-order equations are

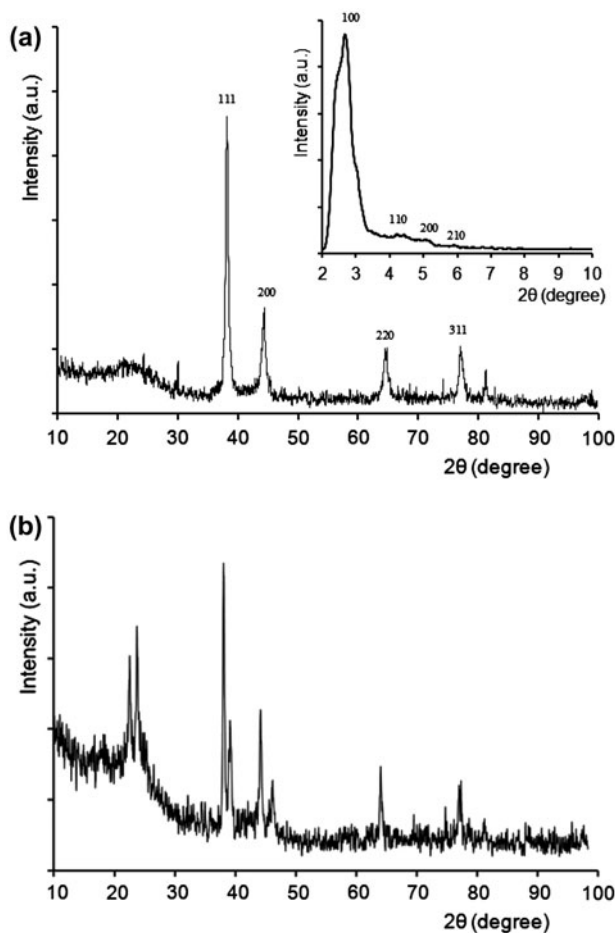


Fig. 1. XRD pattern of the prepared Ag-MCM-41 sample before (a) and after (b) iodide sorption.

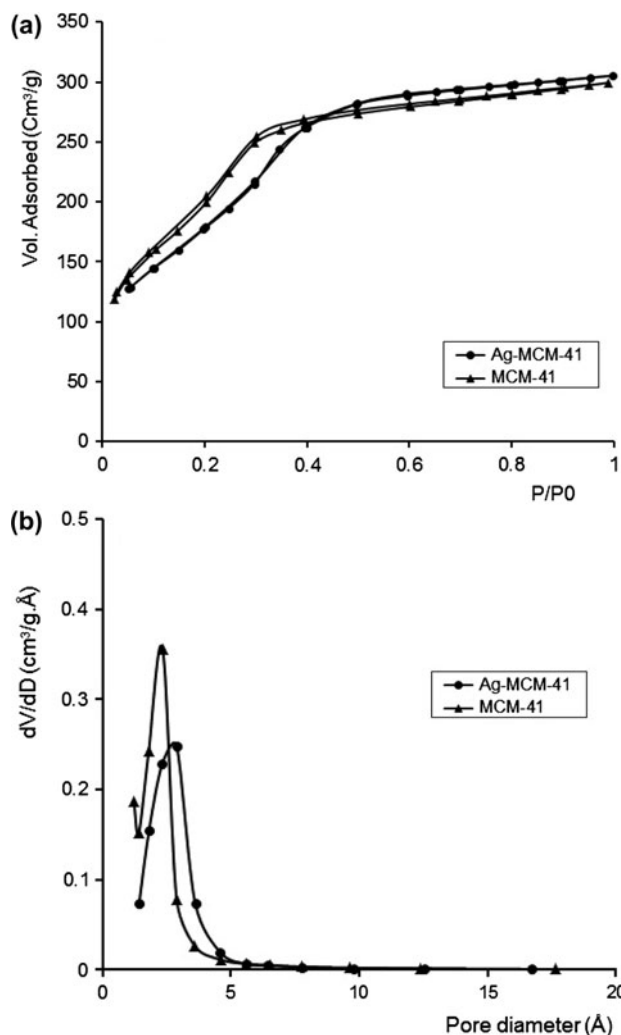


Fig. 2. Nitrogen sorption/desorption isotherms of the MCM-41 and Ag-MCM-41 samples.

Table 1
Physical properties of the MCM-41 and Ag-MCM-41

Sample	Pore volume (mL g ⁻¹)	BET surface area (m ² g ⁻¹)	Pore diameter (nm)
MCM-41	0.46	771.4	2.34
Ag-MCM-41	0.47	697.2	2.88

applied to model the kinetics of iodide adsorption onto Ag-MCM-41. The pseudo-first-order kinetics and the pseudo-second-order kinetics are expressed by Eqs. (4) and (5), respectively [22].

$$\log(q_e - q_t) = \log q_e - \frac{k_1}{2.303} t \tag{4}$$

$$\frac{t}{q_t} = \frac{1}{k_2 q_e^2} + \frac{t}{q_e} \tag{5}$$

where q_e and q_t are the adsorbed metal in mg g⁻¹ on the adsorbent at equilibrium and time t , respectively, k_1 is the constant of first-order adsorption in min⁻¹, and k_2 is the rate constant of second-order adsorption in g mg⁻¹ min⁻¹.

2.4.3. Effect of temperature

The adsorption of iodide ions on the Ag-MCM-41 adsorbent as a function of temperature was investigated.

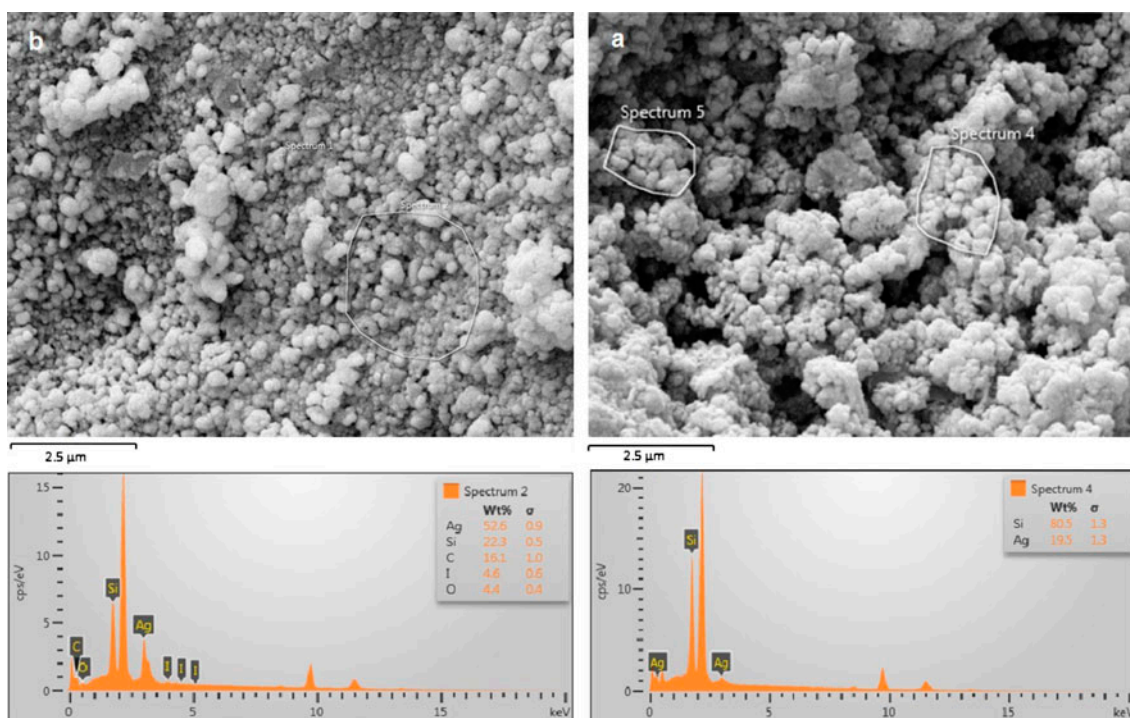


Fig. 3. SEM images and EDX area analysis of the Ag-MCM-41 before (a) and after (b) iodide sorption.

Table 2
Adsorption measurement of iodide on the MCM-41 and Ag-MCM-41

Sample	C _i (mg L ⁻¹)	C _f (mg L ⁻¹)	pH	Contact time (h)	Percent removal (%)
MCM-41	135	135	6.2	5	0
Ag-MCM-41	135	105.9	6.2	5	21.6

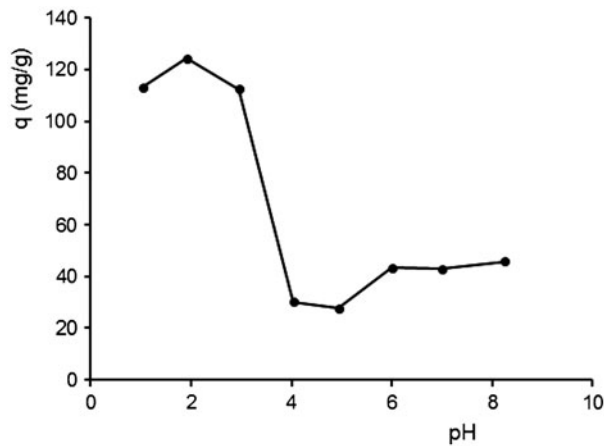


Fig. 4. Effect of pH on iodide sorption onto Ag-MCM-41. Conditions: initial concentration of iodide: $1.2 \times 10^{-2} \text{ mol L}^{-1}$, agitation time: 48 h, and temperature: 25°C.

In batch experiments, 25 mg of the Ag-MCM-41 adsorbent was equilibrated with 25 mL of the solution containing $1.2 \times 10^{-2} \text{ mol L}^{-1}$ of iodide ions at temperatures of 25, 35, 45, 55, and 65°C at pH 2.0.

2.4.3.1. Thermodynamic parameters. For evaluating thermodynamic criteria, the Gibbs free energy (ΔG°) was calculated by the following equation [22]:

$$\ln k_d = \frac{\Delta S^\circ}{R} - \frac{\Delta H^\circ}{RT} \quad (6)$$

where the values of ΔH° (change in enthalpy in J mol^{-1}) and ΔS° (change in entropy in $\text{J mol}^{-1} \text{ K}^{-1}$) are obtained from slope and intercept of $\ln k_d$ versus $1/T$ plots. T is the temperature in K, and R is the universal gas constant ($8.314 \text{ J mol}^{-1} \text{ K}^{-1}$).

The ΔG° is the change in Gibbs free energy in J mol^{-1} , calculated according to the following equation [22]:

$$\Delta G^\circ = \Delta H^\circ - T\Delta S^\circ \quad (7)$$

2.4.4. Adsorption isotherm

In order to determine the relationship between the amount of iodide ions adsorbed on the adsorbent surface and the concentration of remaining metal ions in the aqueous phase, the adsorption isotherm studies were performed. Among various binding models, the

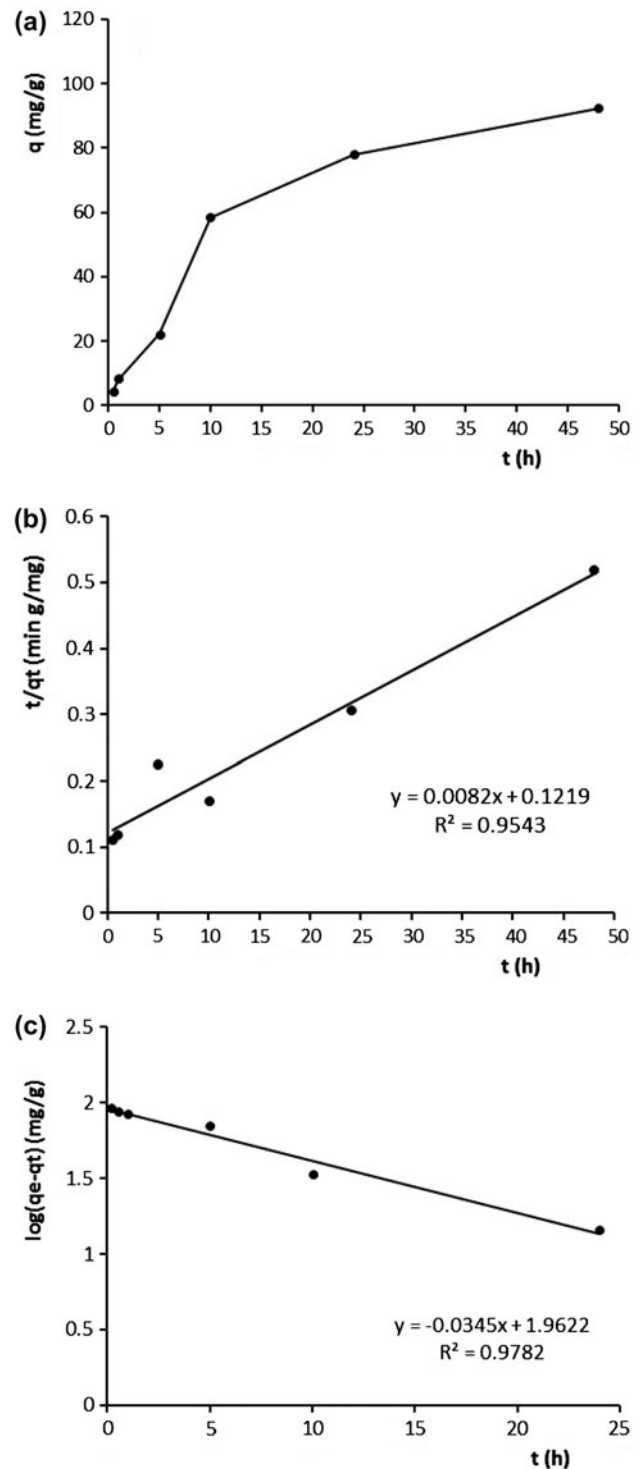


Fig. 5. Sorption kinetics of iodide onto Ag-MCM-41 (a), pseudo-first-order and pseudo-second-order linear plot (b) and (c). Conditions: initial concentration of iodide: $1.2 \times 10^{-2} \text{ mol L}^{-1}$, initial pH: value 2.0, and temperature: 25°C.

Table 3

Kinetic adsorption parameters obtained using pseudo-first-order and pseudo-second-order models

Pseudo-first-order			Pseudo-second-order		
k_1 (min ⁻¹)	q_e (mg g ⁻¹)	R^2	k_2 (g mg ⁻¹ min ⁻¹)	q_e (mg g ⁻¹)	R^2
0.001	91.6	0.978	0.00009	125.0	0.954

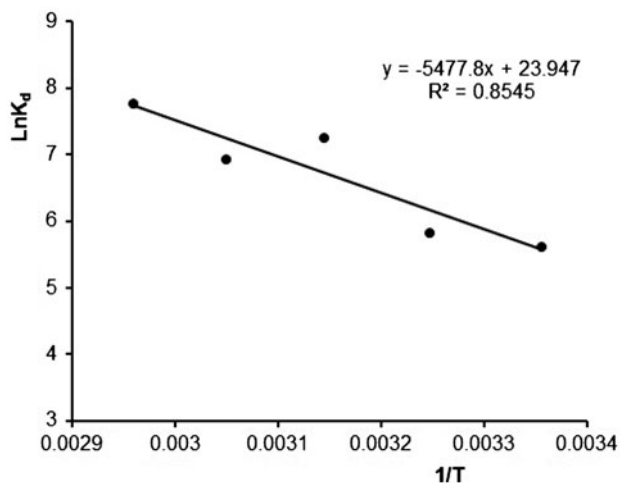


Fig. 6. Plots of $\ln K_d$ vs. $1/T$ for iodide sorption on Ag-MCM-41. Conditions: initial concentration of iodide: 1.2×10^{-2} mol L⁻¹, initial pH value: 2.0, agitation time: 48 h.

Langmuir and Freundlich isotherms have been frequently employed to describe the experimental data of adsorption isotherms. The Langmuir and Freundlich adsorption isotherms are mathematically expressed as Eqs. (8) and (9), respectively [22].

$$\frac{1}{q_e} = \frac{1}{q_{\max}} + \frac{1}{k_1 q_{\max} C_e} \quad (8)$$

$$\ln q_e = \ln k_f + m \ln C_e \quad (9)$$

where q_e (mg g⁻¹) is the amount of analyte bound to the adsorbent, C_e (mg L⁻¹) is the equilibrium concentration of the adsorbate in solution, q_{\max} is the maximum adsorption capacity (mg g⁻¹), and K_f , K_1 , and m are constants for a given adsorbate and adsorbent at a particular temperature.

Table 4

Thermodynamic parameters of iodine adsorption on Ag-MCM-41

ΔH° (kJ mol ⁻¹)	ΔS° (J ⁻¹ mol ⁻¹ K ⁻¹)	ΔG° (kJ mol ⁻¹)					R^2
		298	308	318	328	338	
45.54	0.199	-13.79	-15.78	-17.77	-19.76	-21.75	0.854

2.4.5. Effect of competing anions

The effect of fluoride and chloride anions on the iodide sorption was investigated at a constant concentration of iodide. In batch experiments, 25 mg of the Ag-MCM-41 adsorbent was equilibrated with 25 mL of the solution containing 1.2×10^{-2} mol L⁻¹ of iodide ions with various concentrations of the fluoride and chloride anions (1×10^{-1} , 5×10^{-2} , 1×10^{-2} , 5×10^{-3} , 1×10^{-3} , 5×10^{-4} , and 1×10^{-4} mol L⁻¹).

3. Results and discussion

Fig. 1(a) and (b) are the XRD patterns of the prepared Ag-MCM-41 before and after iodide sorption, respectively. The position of the main diffraction peaks of the Ag-MCM-41 such as 111, 200, 220, and 311 corresponds well to these of silver nanoparticles [23], which is consistent with the presence of silver nanoparticles onto mesoporous MCM-41. The low-angle XRD pattern of the prepared Ag-MCM-41 sample also shows a strong diffraction at 2θ smaller than 3° along with two small peaks that confirm the presence of mesoporous MCM-41 in the prepared sample [24,25]. The positions of the diffraction peaks of the Ag-MCM-41 after iodide adsorption, for example, 23.8° , 25.4° , 39.3° , and 46.3° , matched well with standard JCPDS card No. (00-001-0502) for AgI, which confirms the formation of silver iodide onto mesoporous MCM-41 after iodide adsorption.

The nitrogen adsorption/desorption isotherms and pore size distribution curves of the MCM-41 and Ag-MCM-41 are shown in Fig. 2(a) and (b), respectively. The nitrogen adsorption/desorption isotherms show a typical profile of type IV due to the presence of mesopores in both samples [24,25]. Table 1 shows the BET-specific surface area, total pore volume and pore size changed from 771.4 m² g⁻¹, 0.46 mL g⁻¹, and

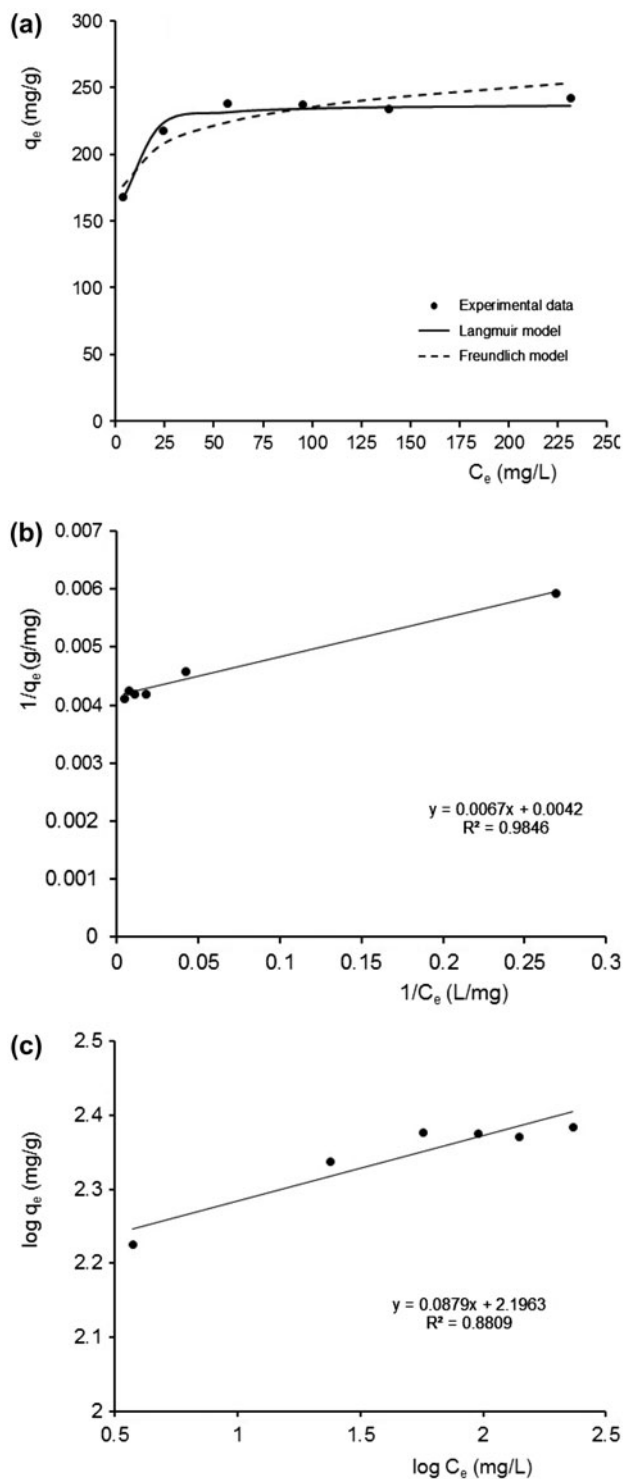


Fig. 7. Sorption isotherms of Ag-MCM-41 for iodide sorption (a), linearized Langmuir and Freundlich plot (b) and (c). Conditions: initial pH value 2.0, agitation time 48 h and temperature 65°C.

2.34 nm for MCM-41 to 697.2 m² g⁻¹, 0.47 mL g⁻¹, and 2.88 nm for Ag-MCM-41, respectively. The results

Table 5

Langmuir and Freundlich isotherm model fitting parameters for iodine

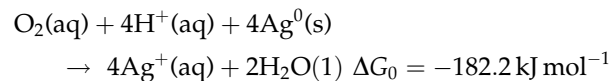
Models	Fitting parameters		
Langmuir	R ²	K _l (L mg ⁻¹)	q _{max} (mg g ⁻¹)
	0.985	0.627	238.1
Freundlich	R ²	K _f (mg g ⁻¹ mg ^{-m} L ^m)	m
	0.881	157.1	0.088

suggested that some of the pores (especially micropores) of MCM-41 were probably blocked by the loading of silver nanoparticles.

Fig. 3(a) and (b) shows SEM images and EDS spectrum patterns of the Ag-MCM-41 before and after iodide sorption, respectively. The EDS spectrum patterns show the strong silicon peak from the mesoporous silicate MCM-41 support. The silver peak is also observed which offers the evidence that silver nanoparticles are loaded on the surface of MCM-41. The weak iodine peak shows that the silver-modified MCM-41 adsorbed iodide ions from aqueous solution.

In preliminary experiments, it was observed that MCM-41 did not have any affinity toward iodide ion (even at long contact times (1–5 h), while Ag-MCM-41 adsorbed iodide ions. The results of preliminary experiments are presented in Table 2. Therefore, the studies were continued on the Ag-MCM-41 sample.

One of the most important factors in sorption studies is the effect of acidity. The iodide uptake was studied at various pH values (1.0–8.0) on the prepared Ag-MCM-41. Results of the experiments are shown in Fig. 4. Iodide sorption on the Ag-MCM-41 was low in pH greater than 4.0, which show a significant competition of OH⁻ ions with iodide ions for the same binding site of sorbent. As SEM results indicated, silver initially exists as metallic silver on the Ag-MCM-41 surface [26]. Therefore, it appears that metallic silver is oxidized to silver ions before iodide precipitation occurred. The metallic silver is oxidized in aqueous solutions according to the following reaction [26]:



The pH_{pzc} value determined of the Ag-MCM-41 was 4.0, and for the pH values lower than pH_{pzc}, the sorbent presents a positive surface charge. This behavior

Table 6

Comparison of iodine adsorption by Ag-MCM-41 in this study with other adsorbents from literatures

Adsorbent	Initial iodide conc. (mg L ⁻¹)	Iodide sorption		Adsorbent dose (g L ⁻¹)	Contact time (h)	pH	Temp. (°C)	Ref.
		%	mg g ⁻¹					
Duolite A-116	510	50	–	5	3	–	25	[29]
Mg–Al-(NO ₃) LHD ^a	342	59	–	20	4	9.2	25	[28]
CaALG-AgCl composite ^b	–	–	139.7	5	48	–	25	[30]
AgAC ^c (1.05 wt% of Ag)	1–200	–	18.2–19.5	1	168	5	–	[26]
Ag-MCM-41	88–352	95–34	166.7–238.1	0.5	48	2	65	This work

^aLayered double hydroxide.^bCalcium alginate-silver chloride composite.^cSilver-impregnated granular activated carbon.

explain the higher sorption amount of the Ag-MCM-41 in pH lower than 4.0. In order to continue the sorption studies, the initial pH was fixed at 2.0.

Fig. 5(a) shows the effect of contact time on the iodide sorption onto Ag-MCM-41. Fig. 5(b) and (c) also shows linear plots of pseudo-first-order and pseudo-second-order models, respectively. The kinetic parameters are listed in Table 3. It shows that the correlation coefficient (R^2) of the pseudo-second-order model is 0.954, less than that of the pseudo-first-order model (0.978). Thus, the latter model is more suitable to predict the kinetics of iodide sorption onto Ag-MCM-41 in the current study. Also the confirmation of pseudo-first-order kinetics indicates that the iodide concentration is involved in the rate-determining step of the sorption process.

The effect of temperature on the sorption of iodide ions onto Ag-MCM-41 is shown by the linear plot of $\ln k_d$ vs. $1/T$ in Fig. 6, and the relative parameters and correlation coefficients calculated from Eqs. 6 and 7 are listed in Table 4. The positive values of ΔH° and the increasing value of k_d with increasing temperature indicate that the sorption of iodide ions onto the Ag-MCM-41 is an endothermic process, and thus, faster adsorption properties, at higher temperature, were obtained. The positive value of ΔS° indicates feasible sorption. It is noticeable that the ΔG° values decrease with increasing temperature, indicating higher spontaneity at higher temperatures. It was found that free energy change for physisorption is generally between -20 and 0 kJ mol⁻¹, the physisorption together with chemisorption within -20 to -80 kJ mol⁻¹, and pure chemisorption in the range from -80 to -400 kJ mol⁻¹ [27]. The calculated ΔG° (-21.8 kJ mol⁻¹ at 338 k) suggests that the sorption processes of iodide on the Ag-MCM-41 could be considered as physisorption together with chemisorption process.

Fig. 7(a) shows the experimental, Langmuir and Freundlich model isotherms. Fig. 7(b) and (c) also shows linear Langmuir and Freundlich plots. The Langmuir isotherm model fitted the experiment data better than Freundlich isotherm model. The Langmuir model is used for homogeneous surfaces with identical binding sites. The values of the fitting parameters and correlation coefficient are shown in Table 5. As seen, the calculated maximum sorption capacity (q_{\max}) was 238.1 mg g⁻¹.

A comparison of Ag-MCM-41 sorbent performance for iodide removal from aqueous solutions with different sorbents reported in the literatures [26,28–30] is given in Table 6. Comparison of q_{\max} values showed that the iodide sorption capacity of the Ag-MCM-41 prepared in our work was higher than that in the

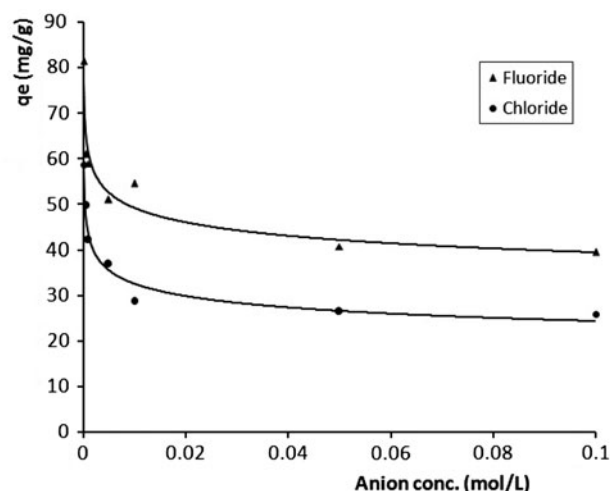


Fig. 8. Effect of the presence of chloride and fluoride on iodide sorption.

previously reported values. The high adsorption affinity of the Ag-MCM-41 is probably due to high affinity of silver loaded onto MCM-41 and also high surface area of Ag-MCM-41 sorbent than other sorbents.

The effect of the coexisting anions of chloride (Cl^-) and fluoride (F^-) on iodide sorption onto Ag-MCM-41 was evaluated (Fig. 8). The results showed that the sorption capacity (q) of iodide was decreased to 25 and 40 mg g^{-1} in the presence of chloride and fluoride, respectively. Considering that iodide concentrations in the contaminated waste streams of interest are at the $\mu\text{g L}^{-1}$ level, the large capacity of the Ag-MCM-41 means that small amounts of this sorbent are required to sequester iodide in nuclear waste leachates for long times while limiting the release of iodide by the solubility control of the AgI solid [31].

4. Conclusion

This work is focused to study the synthesis of a new sorbent (Ag-MCM-41) by the impregnation of mesoporous MCM-41 with silver atoms and its sorption behavior of iodide. The characterization results showed that silver nanoparticles is loaded on the mesoporous MCM-41, after carefully isolated from the mentioned preparation system. The sorption results indicates that under optimum conditions, the maximum sorption values (238.1 mg g^{-1}) comply that the Ag-MCM-41 is an effective adsorbent for iodide.

References

- [1] R.S. Magazinovic, B.C. Nicholson, D.E. Mulcahy, D.E. Davey, Bromide levels in natural waters: Its relationship to levels of both chloride and total dissolved solids and the implications for water treatment, *Chemosphere*. 57 (2004) 329–335.
- [2] M.J. Plewa, E.D. Wagner, S.D. Richardson, A.D. Thruston, Y.T. Woo, A.B. McKague, Chemical and biological characterization of newly discovered iodoacid drinking water disinfection byproducts, *Environ. Sci. Technol.* 38 (2004) 4713–4722.
- [3] S.D. Richardson, Disinfection by-products and other emerging contaminants in drinking water, *TrAC, Trends Anal. Chem.* 22 (2003) 666–684.
- [4] S.D. Richardson, M.J. Plewa, E.D. Wagner, R. Schoeny, D.M. Demarini, Occurrence, genotoxicity, and carcinogenicity of regulated and emerging disinfection by-products in drinking water: A review and roadmap for research, *Mutat. Res./Rev. Mutat. Res.* 636 (2007) 178–242.
- [5] U.V. Gunten, Ozonation of drinking water: Part II. Disinfection and by-product formation in presence of bromide, iodide or chlorine, *Water Res.* 37 (2003) 1469–1487.
- [6] D.F. Sava, M.A. Rodriguez, K.W. Chapman, P.J. Chupas, J.A. Greathouse, P.S. Crozier, T.M. Nenoff, Capture of volatile iodine, a gaseous fission product, by zeolitic imidazolate framework-8, *J. Am. Chem. Soc.* 133 (2011) 12398–12401.
- [7] E.P. Krasavina, S.A. Kulyukhin, L.V. Mizina, N.A. Konovalova, I.A. Rumer, New composite materials containing fine particles of D-elements for localization of molecular radioactive iodine in water coolants of nuclear power plants, *Inorg. Mater. Appl. Res.* 3 (2012) 342–346.
- [8] O.B. Yang, J.C. Kim, J.S. Lee, Y.G. Kim, Use of activated carbon fiber for direct removal of iodine from acetic acid solution, *Ind. Eng. Chem. Res.* 32 (1993) 1692–1697.
- [9] P.K. Sinha, K.B. Lal, J. Ahmed, Removal of radioiodine from liquid effluents, *Waste Manage.* 17 (1997) 33–37.
- [10] G. Fetter, M.T. Olguin, P. Bosch, V.H. Lara, S. Bulbulian, $^{131}\text{I}^-$ sorption from aqueous solutions by nitrated hydrotalcites, *J. Radioanal. Nucl. Chem.* 241 (1999) 595–599.
- [11] S.K. Maiti, S. Dinda, M. Nandi, A. Bhaumik, R. Bhattacharyya, Selective epoxidation of olefins catalyzed by oxodiperoxomolybdenum(VI) complexes immobilized over highly ordered 2D-hexagonal mesoporous silica, *J. Mol. Catal. A: Chem.* 287 (2008) 135–141.
- [12] M.K. Bhunia, S.K. Das, A. Dutta, A. Sengupta, A. Bhaumik, Fine dispersion of BiFeO_3 nanocrystallites over highly ordered mesoporous silica material and its photocatalytic property, *J. Nanosci. Nanotechnol.* 13 (2013) 2557–2565.
- [13] L. Mercier, T.J. Pinnavaia, Access in mesoporous materials: Advantages of a uniform pore structure in the design of a heavy metal ion adsorbent for environmental remediation, *Adv. Mater.* 9 (1997) 500–503.
- [14] M. Puanngam, F. Unob, Preparation and use of chemically modified MCM-41 and silica gel as selective adsorbents for Hg(II) ions, *J. Hazard. Mater.* 154 (2008) 578–587.
- [15] P.A. Mangrulkar, S.P. Kamble, J. Meshram, S.S. Rayalu, Adsorption of phenol and o-chlorophenol by mesoporous MCM-41, *J. Hazard. Mater.* 160 (2008) 414–421.
- [16] P. Selvam, S.K. Bhatia, C.G. Sonwane, Recent advances in processing and characterization of periodic mesoporous MCM-41 silicate molecular sieves, *Ind. Eng. Chem. Res.* 40 (2001) 3237–3261.
- [17] C.F. Cheng, W. Zhou, D.H. Park, J. Klinowski, M. Hargreaves, L.F. Gladden, Controlling the channel diameter of the mesoporous molecular sieve MCM-41, *J. Chem. Soc., Faraday Trans.* 93 (1997) 359–363.
- [18] H. Sepehrian, J. Fasihi, M. Khayatzaheh Mahani, Adsorption behavior studies of picric acid on mesoporous MCM-41, *Ind. Eng. Chem. Res.* 48 (2009) 6772–6775.
- [19] H. Chen, Y. Wang, F.H. Yang, R.T. Yang, Desulfurization of high-sulfur jet fuel by mesoporous π -complexation adsorbents, *Chem. Eng. Sci.* 64 (2009) 5240–5246.
- [20] Y. Yang, Y. Chun, G. Sheng, M. Huang, pH-dependence of pesticide adsorption by wheat-residue-derived black carbon, *Langmuir* 20 (2004) 6736–6741.
- [21] A. Aziz, M.S. Ouali, E.H. Elandaloussi, L.C. De Menorval, M. Lindheimer, Chemically modified olive stone: A low-cost sorbent for heavy metals and basic dyes removal from aqueous solutions, *J. Hazard. Mater.* 163 (2009) 441–447.

- [22] R. Cheraghali, H. Tavakoli, H. Sepehrian, Preparation, characterization and lead sorption performance of alginate-SBA-15 composite as a novel adsorbent, *Sci. Iran.* 20 (2013) 1028–1034.
- [23] E.J. Park, S.W. Lee, I.C. Bang, H.W. Park, Optimal synthesis and characterization of Ag nanofluids by electrical explosion of wires in liquids, *Nanoscale Res. Lett.* 6 (2011) 223–233.
- [24] C.T. Kresge, M.E. Leonowicz, W.J. Roth, J.C. Vartuli, J.S. Beck, Ordered mesoporous molecular sieves synthesized by a liquid-crystal template mechanism, *Nature* 359 (1992) 710–712.
- [25] J.S. Beck, J.C. Vartuli, W.J. Roth, M.E. Leonowicz, C.T. Kresge, K.D. Schmitt, C.T.W. Chu, D.H. Olson, E.W. Sheppard, S.B. Mccullen, J.B. Higgins, J.L. Schlenker, A new family of mesoporous molecular sieves prepared with liquid crystal templates, *J. Am. Chem. Soc.* 114 (1992) 10834–10843.
- [26] J.S. Hoskins, T. Karanfil, S.M. Serkiz, Removal and sequestration of iodide using silver-impregnated activated carbon, *Environ. Sci. Technol.* 36 (2002) 784–789.
- [27] M.M. Rao, G.P.C. Rao, K. Seshiah, N.V. Choudary, M.C. Wang, Activated carbon from *Ceiba pentandra* hulls, an agricultural waste, as an adsorbent in the removal of lead and zinc from aqueous solutions, *Waste Manage.* 28 (2008) 849–858.
- [28] L. Kentjono, J.C. Liu, W.C. Chang, C. Irawan, Removal of boron and iodine from optoelectronic wastewater using Mg–Al(NO₃) layered double hydroxide, *Desalination* 262 (2010) 280–283.
- [29] R. Lokhande, P. Singare, S. Parab, Application of radioactive tracer technique to study the kinetics of iodide ion-isotope exchange with strongly basic anion-exchange resin Duolite A-116, *Radiochemistry* 50 (2008) 642–644.
- [30] H. Zhang, X. Gao, T. Guo, Q. Li, H. Liu, X. Ye, M. Guo, Z. Wu, Adsorption of iodide ions on a calcium alginate-silver chloride composite adsorbent, *Colloids Surf. A* 386 (2011) 166–171.
- [31] A.L. Pishko, S.M. Serkiz, K.E. Zeigler, A.M. Rao, Removal and sequestration of iodide from alkaline solutions using silver doped carbon nanotubes, *J. South Calif. Acad. Sci.* 9 (2011) 37–42.